ELSEVIER

Journal of Nuclear Materials 278 (2000) 85–95

journal of nuclear materials

www.elsevier.nl/locate/jnucmat

Investigation on oxygen controlled liquid lead corrosion of surface treated steels

G. Müller *, G. Schumacher, F. Zimmermann

Forschungszentrum Karlsruhe GmbH, Institut für Hochleistungsimpuls- und Mikrowellentechnik, IHM, Postfach 3640, 76021 Karlsruhe, Germany

Received 11 June 1999; accepted 10 August 1999

Abstract

A low alloyed martensitic steel Fe9Cr (OPTIFER IVc) and an austenitic steel 16Cr15Ni (1.4970) were exposed to liquid lead to examine their suitability as structural material for lead cooled accelerator driven subcritical actinide burners. The surface of part of the steel specimens was restructured and that of another part was alloyed with Al by treatment with high power pulsed electron beams. A corrosion test stand was constructed containing liquid lead under oxygen control at 550°C. Steel specimens were examined after 800, 1500 and 3000 h of exposure. For austenitic steel lower corrosion effects were observed especially when the surface was treated by the electron beam. No corrosion attack could be seen at all on both steels after alloying Al into a surface layer of 10 μm depth.

1. Introduction

Recently, promising proposals were discussed on accelerator driven subcritical systems (ADS) for energy production and as actinide burners [1]. These concepts include liquid metal cooling systems on the basis of Pb–Bi or Pb. However, corrosion problems with steel arise in using such coolants. Severe intergranular attack was observed for AISI 316 steel in liquid lead. Corrosion effects in the 100 μm range occurred in ferritic Fe–Cr steels between 575°C and 750°C after 3250 h of exposure [2]. Compatibility tests with ferritic steels were reported which revealed that corrosion attack can be minimized if an oxide layer exists on the steel surface [3,4].

The highest solubility in lead is that of Ni for which the phase diagram [5] shows 2 at.% at 550°C. The respective phase diagrams for Cr and Fe give reasonable values only for temperatures above 1000°C. Values of 1 at.% Cr and 0.15 at.% Fe can be obtained at 1200°C [5]. Model calculations provide solubilities of about 0.2 at.% Cr and 10^{-3} at.% Fe at 600°C [6]. Contradictory values are given for the solubilities of Cr and Fe by Asher et al. [3] that amount to 6×10^{-4} and 8×10^{-4} at.%, respectively at 700°C. Since all the solubilities vary with temperature, transport processes will take place which live from the higher solubility at high temperatures and precipitation at low temperatures. A temperature difference of 150°C is about typical for lead cooling loops. Therefore already small solubilities can lead to heavy corrosion effects with high flow velocities, in the range of 1 m/s, and long exposure times.

One way to slow down corrosion of metals in liquid Pb would be to use metals with no or very low solubility in lead. Those metals are W with a solubility of <0.0056 at.% and Mo with <0.011 at.% at 1200°C [7]. Molybdenum was reported to be highly resistant, even at 1000°C [3]. Good results were obtained also with Fe–Cr alloys containing 8 at.% Al that allow formation of a protective alumina scale also at low oxygen potentials [3]. Other experiments [8] employing an Fe aluminide layer on MANET steel, which was oxidized before the experiment, resulted in no corrosion attack in liquid Pb–17Li after 10 000 h at 450°C. Thermodynamic investigations of Al–Fe alloys [9] showed the

* Corresponding author. Tel.: +49-7247 82 4669; fax: +49-7247 82 4874.

E-mail address: georg.mueller@ihm.fzk.de (G. Müller).

0022-3115/00/$ - see front matter
PII: S0022-3115(99)00211-1

possibility that a self-healing of the alumina scale can take place if the kinetics of the process is high enough. Gromov et al. [4] and Markov [10] stabilized the oxide layer by maintaining an oxygen concentration of 10^{-6} at.% in liquid Pb or Pb–Bi with an oxygen control system.

An overview of the corrosion behavior of two different austenitic steels in a loop with liquid lead at 550°C as a function of oxygen concentration after 3000 h of exposure is presented in Fig. 1 [10]. At oxygen concentrations below 10^{-7} at.% in lead, corrosion is determined by solution of alloy components in steel. It increases strongly with decreasing oxygen content. Above 10^{-6} at.% oxygen concentration corrosion is caused by oxidation of the surface that on the other hand protects the steel from dissolution of alloying components. No clear statement about the corrosion behavior can be given for the transition zone between 10^{-6} and 10^{-7} at.% oxygen, in which dissolution as well as oxidation could be possible. From this discussion it becomes obvious that it is necessary to measure and control the oxygen concentration exactly, to keep the conditions of the liquid lead in a range of low corrosion effects. After a certain time period, oxygen in Pb or Pb–Bi will be depleted by oxide formation on the surface of the structural steel and thus the conditions will shift to the region with low oxygen concentration and hence strong corrosion effects, if there would be no oxygen control.

In experiments on surface treatment by a pulsed electron beam with the GESA (Gepulste Elektronenstrahlanlage) installation [11], it is observed that the formation of protective oxide scales can be improved by such treatment. During the treatment a thin surface layer melts and solidifies rapidly. By the same process, a metal that is precipitated on the surface can be alloyed into the molten layer. Both methods will be applied in this work to examine, whether the corrosion resistance of steels in liquid lead can be improved.

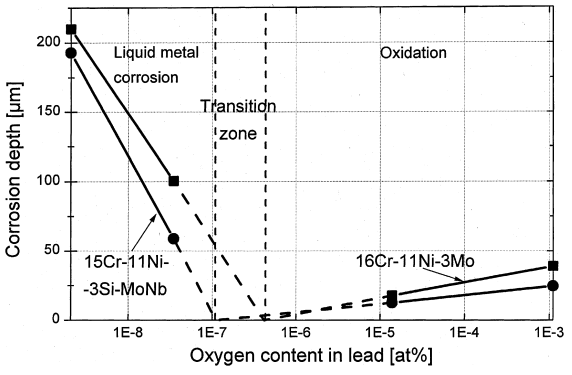

Fig. 1. Corrosion behavior of steels in flowing lead after 3000 h at 550°C, from [10]. Oxide layer is Me_3O_4 type.

2. Conditions for protective oxide scale formation

The concentration of oxygen in lead which is necessary for the protective oxide scale formation on steel structures, may be controlled by solid electrolyte cells that measure and feed oxygen into the liquid lead or lead–bismuth. Such cells are sophisticated and require a special know-how to build them. Another possibility is the control by an atmosphere with a definite oxygen partial pressure that determines the chemical potential of oxygen within the liquid metal bath. To prevent PbO precipitation and to support Fe_3O_4 formation, the following conditions must be established:

$$2\Delta_f G^0_{PbO} > RT \ln p_{O_2} > 0.5\Delta_f G^0_{Fe_3O_4}. \quad (1)$$

The standard values $\Delta_f G^0$ of the Gibbs energies of formation are known for the oxides in question and with these values the equilibrium oxygen partial pressure region that retains the stable conditions can be determined. The easiest way to do this is to draw a diagram that contains oxygen potentials of the relevant oxides PbO, NiO, Fe_3O_4 and Cr_2O_3 and the lines for constant oxygen partial pressures and constant p_{H_2}/p_{H_2O} ratios as a function of temperature. The latter will be used to control the oxygen potential as follows:

$$p_{O_2} = \frac{p^2_{H_2O}}{p^2_{H_2}} \exp \frac{2\Delta_f G^0_{H_2O}}{RT}. \quad (2)$$

The diagram in Fig. 2 demonstrates in which region the stable conditions exist and how they can be established. The ordinate shows the chemical potential of oxygen, the abscissa the temperature. Dashed lines in the diagram represent the isobars of the oxygen partial pressure and the lines of constant p_{H_2}/p_{H_2O} ratios in the gas atmosphere above the oxidizing species or above the liquid lead that dissolved oxygen, respectively. The important region in the diagram is the one between the lines of the oxygen potential for PbO and Fe_3O_4 in the temperature regime of 400–550°C.

For working conditions with reduced corrosion we have to select a field of oxygen partial pressures, the lines of which would not cross the PbO- and Fe_3O_4-lines within the temperature regime of 400–550°C. Lines of constant p_{H_2}/p_{H_2O} ratios within the borders of this field show the ratios that must be established to maintain the appropriate oxygen partial pressures.

If we choose a p_{H_2}/p_{H_2O} ratio of 0.4 we will attain $p_{O_2} \approx 10^{-25}$ at 550°C and $p_{O_2} \approx 10^{-29}$ at 400°C. At both temperatures we still form iron oxide and no PbO in the case of stagnant Pb. If we consider a liquid metal loop, there will be no equilibration across the temperature region via the p_{H_2}/p_{H_2O} ratio but through the oxygen dissolved in Pb (Pb/Bi). In this case we have to consider the variation of the oxygen potential for a constant

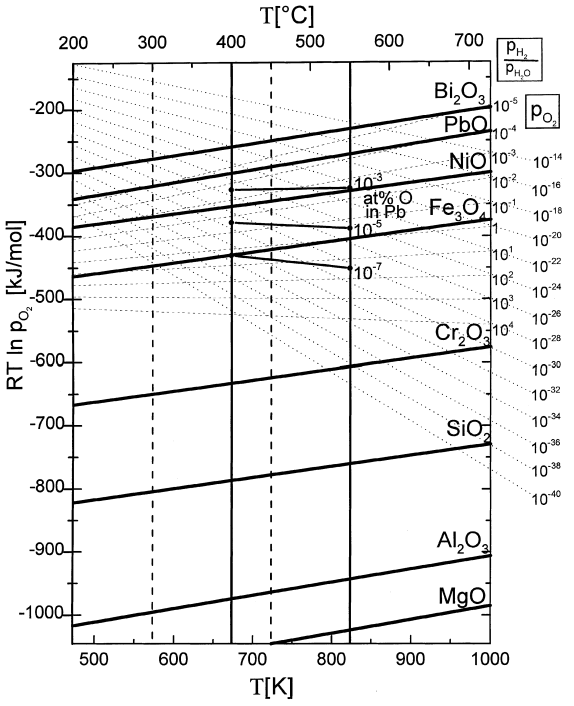

Fig. 2. Oxygen potential diagram with PbO, Fe_3O_4 and other oxides of interest containing lines of constant oxygen partial pressures and H_2/H_2O ratios. Loop temperature regions are marked for Pb by solid, and Pb–Bi by dashed vertical lines. Lines of constant oxygen concentration are drawn in the Pb loop region for 10^{-7}, 10^{-5} and 10^{-3} at.%.

oxygen concentration throughout the considered temperature region between 400°C and 550°C.

For calculation of the oxygen concentration c_O related to an oxygen partial pressure p_{O_2} we need to know the activity coefficient γ_0 at the phase boundary to PbO, which we get from the following relation for the oxygen activity a_O in lead:

$$a_O = \gamma_0 c_O = \frac{c_O}{c_{O,s}} = \left(\frac{p_{O_2}}{p_{O_2,s}}\right)^{1/2}. \quad (3)$$

The suffix (s) indicates the values that correspond to saturation conditions at which the activity becomes unity.

With values for the saturation concentration of oxygen in lead of 4×10^{-2} at.% at 550°C and 7.5×10^{-3} at.% at 400°C [5], equilibrium oxygen concentrations in the range 400–550°C were calculated and drawn in Fig. 2. The solid vertical lines at 400°C and 550°C mark the operating range for a lead cooled loop and the dashed lines at 300°C and 450°C the range for a lead–bismuth coolant. The lines of constant oxygen concentrations indicate safe regions with 10^{-3}–10^{-5} at.% oxygen for the high temperature Pb loop and 10^{-4}–10^{-6} at.% for the low temperature Pb–Bi loop. Activity coefficients for Pb and Pb–Bi do not differ much in the region above about 50 at.% Pb [10]. Therefore, the values calculated here for Pb can be extrapolated for Pb–Bi as an approximation.

The diagram in Fig. 2 also shows the advantage of controlling the oxygen partial pressure by the p_{H_2}/p_{H_2O} ratio. It would not be possible with an oxygen partial pressure of 10^{-25} bar to replace oxygen that was used for oxidation of the surface of the specimens in lead. However, with a p_{H_2}/p_{H_2O} ratio of 0.4 it is easy to replace the oxygen. With a gas flow of 200 cm^3/min, it is possible to provide 10 cm^3 O_2/min which corresponds to about 1000 cm^2 of a Cr_2O_3 layer of 1 μm thickness. With the same gas flow, delivery of the oxygen amount necessary for solution of 10^{-6} at.% oxygen in 1000 cm^3 Pb takes about 1 s. Therefore, the controlling step is only the uptake of oxygen from the gas phase. Thus, not only small and medium loops can be managed by controlling them via the p_{H_2}/p_{H_2O} ratio in the gas phase, if one could deliver the available oxygen through the surface to the lead, e.g. by bubbling.

3. Experimental

3.1. The GESA facility

The surface treatment of the steel was carried out with the GESA facility [11]. GESA is a new pulsed electron beam facility that consists of a high voltage generator with a pulse duration control unit, a multipoint explosive emission cathode, a controlling grid and an anode which form a triode. The kinetic energy of the beam electrons can be varied in the range of 50–150 keV, with a beam power density up to 2 MW/cm^2 at the target and a pulse duration up to 40 μs. The important parameters for the melting process like electron energy, power density and pulse duration can be chosen independent of each other. The energy density absorption of the target is up to 80 J/cm^2, which is sufficient to melt metallic materials adiabatically up to a depth of 10–50 μm. The beam diameter is 6–10 cm and this is the area of surface melting by applying one single pulse. Due to the high cooling rate in the order of 10^7 K/s, very fine grained or even amorphous structures develop during solidification of the molten surface layer.

3.2. Materials

Samples of the martensitic steel OPTIFER IVc and of the austenitic steel 1.4970 were prepared for the corrosion tests. Table 1 shows the compositions of the steels. The specimens are small plates of $15 \times 10 \times 2$ mm^3 dimension. Three conditions of specimens are provided:

Table 1
Chemical composition of OPTIFER IVc and 1.4970 in at.%

	C	Si	Mn	P	S	Cr	V	Ni	Mo	Ti	W	Ta
OPTIFER IVc	0.56	0.02	0.58	0.005	0.009	9.99	0.28	–	–	–	0.30	0.02
1.4970	0.46	0.89	1.91	0.012	0.009	16.5	–	13.8	0.66	0.43	–	–

(a) original OPTIFER and 1.4970 steels,
(b) OPTIFER and 1.4970 steels after surface treatment by a pulsed electron beam,
(c) OPTIFER and 1.4970 steels after surface alloying with Al by a pulsed electron beam.

The original steel specimens were polished to improve the conditions for analysis of the corrosion effects. This was not necessary for the electron pulse treated specimens, because the treatment effects a smooth surface. The very fine grained structure of the rapid solidified melt layer is a suitable basis for the formation of protective oxide scales with good adhesion [11]. The micrograph of the cross-section perpendicular to the surface of a treated OPTIFER steel specimen is presented in Fig. 3. After etching no structural details are visible in the solidified melt region on top of the coarse grained base material.

Surface alloying of the steel specimens was done by applying the electron pulse to the surface covered with a 18 μm thick Al foil. The micrograph of the cross-section is identical to that in Fig. 3. During surface melting 20–25% of the aluminum is dissolved in the melt layer, the remainder evaporates. The Al-concentration profile perpendicular to the surface is shown in Fig. 4. It is obtained by analysis of the cross-section with an ECON 3,4 O detector attached to the scanning electron microscope (SEM) AMR 1000 (Leitz, Wetzlar). The EDAX DX-4 eDX ZAF system was used for the calculation of the concentrations by employing the standardless method. The analysis shows, that Al penetrates into the steel within the molten surface layer. The concentration profile is not typical for a diffusion process, but for a distribution by turbulences in the melt. The obtained structure consist of two phases, which contain different Al concentrations (8–20 at.%) but have the same Cr content.

The structural changes due to melting and rapid solidification of the GESA-treated alloys are examined by X-ray diffraction using Cu $K\alpha_1$ radiation ($\lambda = 154.06$ pm) and a Si standard. The patterns are recorded in Fig. 5. The upper patterns represent the structure of original OPTIFER containing the major α-Fe peaks (ICPDS 6–696). The origin of the peak at $2\Theta = 57°$ could not be resolved. The patterns in the middle are those of the rapid solidified melt layer after electron pulse treatment. It shows the same peaks but with some preferential orientation. The unknown peak at 57° disappeared while another came up at $2\Theta = 53.6°$ which is also unknown. All the peaks are slightly shifted to higher angles ($2\Theta = 44.64°$ for the (1 1 0) peak) probably due to the rapid solidification, resulting in a lattice constant of 287.07 pm as compared to 287.10 pm for Fe10Cr from the literature [12]. The lower pattern is obtained from OPTIFER steel alloyed with Al by electron pulse melting. It contains peaks that can be ascribed to α-Fe(Al), αFe(Cr) and to AlFe as well. The lattice constants are 286.63–290.9 pm (depending on the Al concentration) [9], 287.10 and 290.9 pm [12], respectively. From the data of the (1 1 0) peak a value of 289.05 pm is obtained which corresponds to an Al concentration of about 16 at.% [9]. The small peaks at $2\Theta = 31.0°$ and 81.7° are close to the angles at which

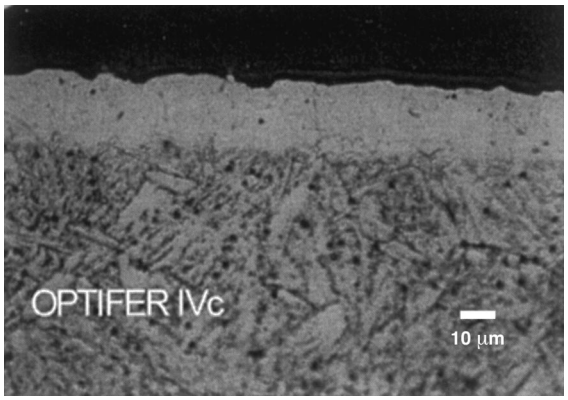

Fig. 3. Optical micrograph of the cross-section of OPTIFER after GESA treatment. The bright region on top is the molten layer.

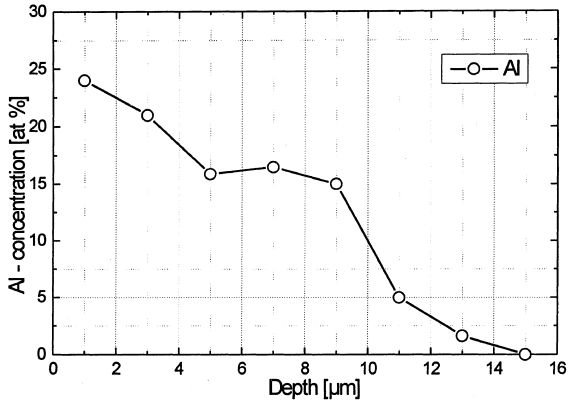

Fig. 4. Concentration profile of Al within the alloyed surface layer of the OPTIFER specimen F3.

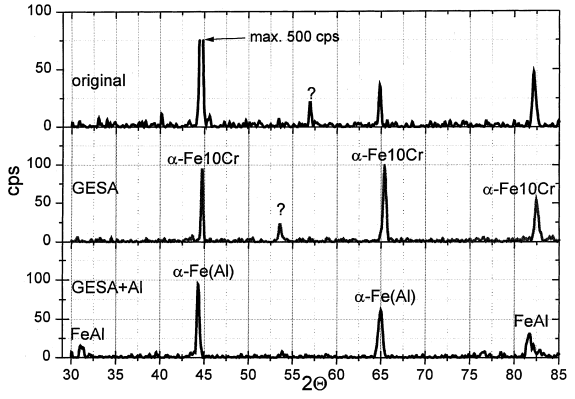

Fig. 5. X-ray diffraction patterns of OPTIFER in the original state, after GESA treatment and after surface alloying of Al.

peaks for Fe_3Al are expected (30.85° and 81.3°), but the existence of this phase can be excluded because of the investigations in [9]. A fit for FeAl disagrees slightly more with 2Θ values of 30.71° for the (1 0 0) peak and 80.87° for the (2 1 1) peak. Thus, the determination of the second phase is doubtful all the more the influence of the dissolved Cr is not known.

3.3. Corrosion tests

A corrosion test stand was built up with control of the oxygen potential via the p_{H_2}/p_{H_2O} ratio in the gas phase as described above. Fig. 6 shows a scheme of this equipment. The reactor is a quartz tube inside a furnace that is controlled at 550°C. A mixture of Ar and Ar–5%H_2 allows the adjustment of the hydrogen concentration in the gas. The water vapor is added by passing the gas through water of a definite temperature. The maximum hydrogen concentration that can be introduced is 5%, which is high enough and well below the lower explosion limit. In the actual experiments, the flow of Ar is 200 cm^3/min and that of Ar–5%H_2 is 16 cm^3/min which gives a p_{H_2}/p_{H_2O} ratio of 0.4 at a water temperature of 7.4°C. The lead in the furnace is not flowing but stagnant and contains 10 crucibles which can take 10 metal specimens. Each crucible is filled with 40 g of high purity lead. The ratios of gas flows are controlled and the partial pressure of water vapor is measured before and behind the furnace. The gas passes also through an oxygen partial pressure measuring system after leaving the furnace.

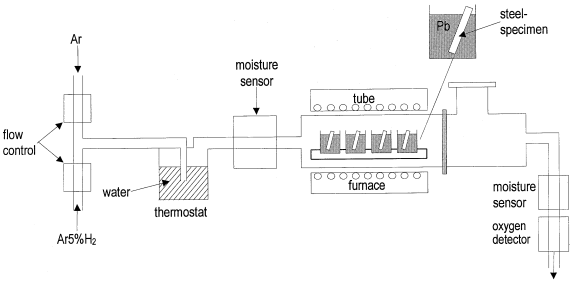

Fig. 6. Corrosion test stand with stagnant liquid lead.

The maximum test time up to now is 3000 h. The samples immerge about 1 cm deep into the liquid lead during the test. The adherent lead is not removed from the specimen surface after the test to conserve the oxide scale. Specimens are examined by cutting them perpendicular to the surface and looking at the cross-section by optical microscopy and SEM combined with an EDX (energy dispersive X-ray analysis) analyzer. The SEC (standardless element concentration) factor for oxygen was estimated by a reversed ZAF-calculation from polished Al_2O_3 and ZrO_2 ceramics covered with the same carbon coating as that on the analyzed specimens. Examinations are carried out after 800, 1500 and 3000 h of exposure.

The oxide scale grown at the surface of the specimens is also analyzed by X-ray diffraction. Because the specimens are difficult to clean from adhering lead, the analysis is done with specimens which were exposed to the controlled atmosphere in the furnace close to the lead crucibles. These specimens show the same features and oxide scale structure as they are observed with those in lead. However, the growth rate of the magnetite scale is enhanced by a factor of 2–3 in the gas atmosphere.

4. Results

After the corrosion test in liquid lead of 550°C in controlled Ar–H_2/H_2O-atmosphere, the specimens are taken from the test stand for metallographic examination and concentration analysis. Specimens and test data are listed in Table 2.

The cross-section of the original OPTIFER steel specimen F1 after exposure is presented in Fig. 7a together with the concentration profiles that are recorded as a function of the distance from the original specimen surface. The micrograph of the cross-section shows the typical corrosion attack with three different zones. The zone at the top, that ends at the original specimen surface, consists of magnetite without appreciable Cr concentration. It is obviously brittle, because many defects exist caused by spallation of scale parts. The layer in the middle contains Cr–Fe spinel that roots in the pore belt. At some places the spinel layer is also missing, an effect that is more pronounced at other places of the specimen. In the interior, an oxygen diffusion zone can be observed in which oxides precipitate along the grain boundaries.

Table 2
Materials and test data after maximum exposure to lead at 550°C containing 8×10^{-6} at.% oxygen[a]

Material data			Test data			
Spec. No.	Type	Treatment	t_{tot} (h)	Mag. scale (μm)	Sp. zone (μm)	Diff. zone (μm)
F1	OPTIFER	Original	3000	20	15	10
F2		e-pulse	3000	16	15	8
F3		Al-alloyed	1500	None	None	None
A1	1.4970	Original	3000	10	6	12[b]
A2		e-pulse	3000	6	6	3[b]
A3		Al-alloyed	1500	None	None	None

[a] mag. = magnetite; sp. = Fe (Fe, Cr)$_2$ O$_4$; e-pulse = pulsed electron beam, GESA; diff. = diffusion.
[b] Including grain boundary penetration.

The concentration profile in Fig. 7(a) indicates the zone structure also. Both oxide layers are hypostoichiometric with O/M ratios of around 1 for the metals that form oxides. Only at the scale surface the O/M ratio was higher and reached a value of 1.3. The concentration in the diffusion zone is about 10% of that in the magnetite scale. Peaks in this zone indicate spinel precipitation in a grain boundary. Within the spinel zone, the Cr concentration reaches a maximum of twice the concentration in the bulk due to Fe depletion caused by the magnetite scale formation. Specimen F2 that was treated by an electron pulse before the test shows the same features as the non-treated specimen F1. Different is the size of the magnetite scale which is smaller and more compact than on the untreated surface but is also partially spalled-off, Fig. 7(b). Furthermore, the spinel layer is completely retained without spallation.

For demonstration of the effect of Al-alloying into the surface, specimen F3 is alloyed with Al by electron pulse treatment only on one half of the surface. There is no corrosion attack visible in the alloyed part at all after 1500 h exposure to liquid lead at 550°C, Fig. 8. Also, the concentration profiles do not give any indication of an interaction between lead or oxygen and the alloyed specimen part. Only the unalloyed part of the surface to the right is covered with thick oxide scales. It is obvious from this micrograph that the Fe–Cr spinel layer ends at the original specimen surface.

The development of the magnetite scale is also examined by X-ray diffraction. Fig. 9(a) presents diffraction patterns of the OPTIFER specimen F1 after exposure to the atmosphere in the test furnace for times up to 500 h. The peaks of α-Fe disappear already after 110 h and get replaced by magnetite and/or spinel peaks marked by 'M' (magnetite). Intensity changes of those peaks during exposure indicate a reorientation of crystals in the oxide scale. Besides the magnetite peaks there are several others marked by 'H' (hematite) that only can be fitted by data of Fe_2O_3 and (Fe, Cr)$_2$O$_3$ (ICPDS 34-140 and 2-1357). Those peaks are steadily increasing and indicate a growing part of this phase on the scale surface. Scale development on the electron pulse treated OPTIFER steel specimen F2 shows essentially the same features as observed on the original specimen F1, Fig. 9(b). The only difference is in the starting material (0 h), where a reoriented structure can be seen as described before.

A completely different behavior is visible from the X-ray patterns of the surface of the specimen F3 alloyed with Al at the surface, Fig. 9(c). Even after 500 h of oxidation there exist no peaks of magnetite, spinel or Al_2O_3. The alumina layer is still too small to give clear peaks and the peaks of α-Fe(Al) are not diminished. The only change is an intensity shift between the two major peaks probably because of thermal restructuring.

The structure of the oxidation region on the original 1.4970 steel specimen A1 is similar to that on OPTIFER steel with layers of magnetite and Fe–Cr spinel and an oxygen diffusion zone in the interior. However, the Fe–Cr spinel zone contains Pb and oxygen penetrates along grain boundaries up to 20 μm deep into the metal matrix, Fig. 10(a). Remarkable is the strong depletion of Ni within the spinel zone, that was observed in the first inspection after 800 h of exposure. It develops probably already in the first hours and does not change any more. The oxygen diffusion zone is much smaller in the electron pulse treated specimen A2 than in A1, because it does not show the deep grain boundary attack, Fig. 10(b). The Pb-containing spinel layer looks tighter and smaller and is strongly depleted in Ni. Most of the magnetite layer got also lost. There is no attack observable from the concentration profiles of the Al-alloyed austenitic specimen A3, Fig. 11. No oxygen penetration through the surface and no Ni-depletion took place. The micrograph does not show any signs of corrosion.

X-ray diffraction analysis of austenitic specimens did not result in new findings and is not presented here. The only difference to the OPTIFER material is the lower growth rate of the magnetite peaks, because after 500 h there are still Fe peaks visible.

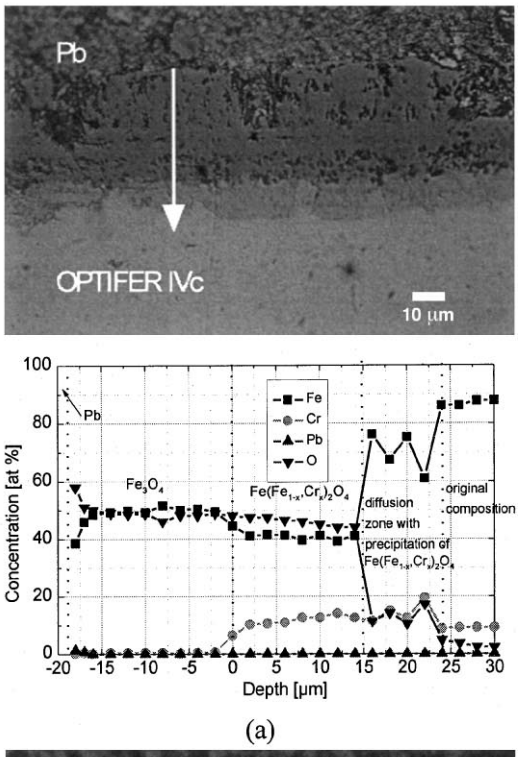

Fig. 7. SEM of cross-sections of OPTIFER specimens and EDX concentration profiles (at arrow position) after 3000 h at 550°C: (a) original, F1, (b) GESA treated, F2.

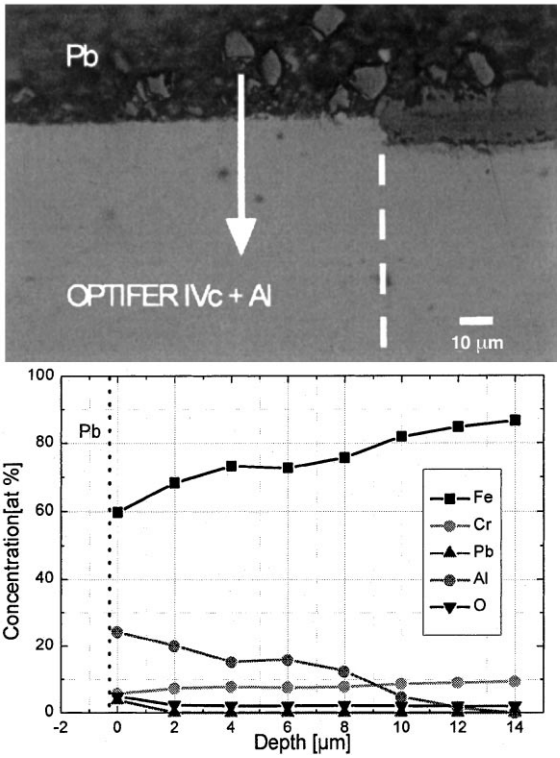

Fig. 8. SEM of the cross-section of OPTIFER specimen F3 alloyed with Al on the left surface part and EDX concentration profiles through the alloyed surface layer (at arrow position) after 1500 h at 550°C.

5. Discussion of results

The examination of the corrosion tests with OPTIFER and 1.4970 steel specimens proves that the behavior of these materials in liquid lead changes with the treatment on the surface region. Large oxidation layers are formed on the unalloyed OPTIFER steel surface. They are thinner on 1.4970 steel. No oxidation attack can be observed on both steel surfaces alloyed with Al. Three distinct oxidation zones are developed on the unalloyed steel surface, an outer magnetite scale which is placed on top of the original surface, an $Fe^{2+}(Fe^{3+}_{1-x}Cr^{3+}_{x})_2O_4$ spinel layer that lies beneath the original surface and below this one, and beyond a pore belt an oxygen diffusion zone with spinel formation along grain boundaries, see Fig. 12. From the concentration curves the Cr fraction x results in about 0.3 for OPTIFER and in a maximum value of 0.6 for 1.4970 steel.

The stratified oxide layer structure agrees with descriptions by Hauffe [13] and Talbot [14] for oxidation of steels in air at temperatures below 570°C. The only difference to our results obtained by experiments in

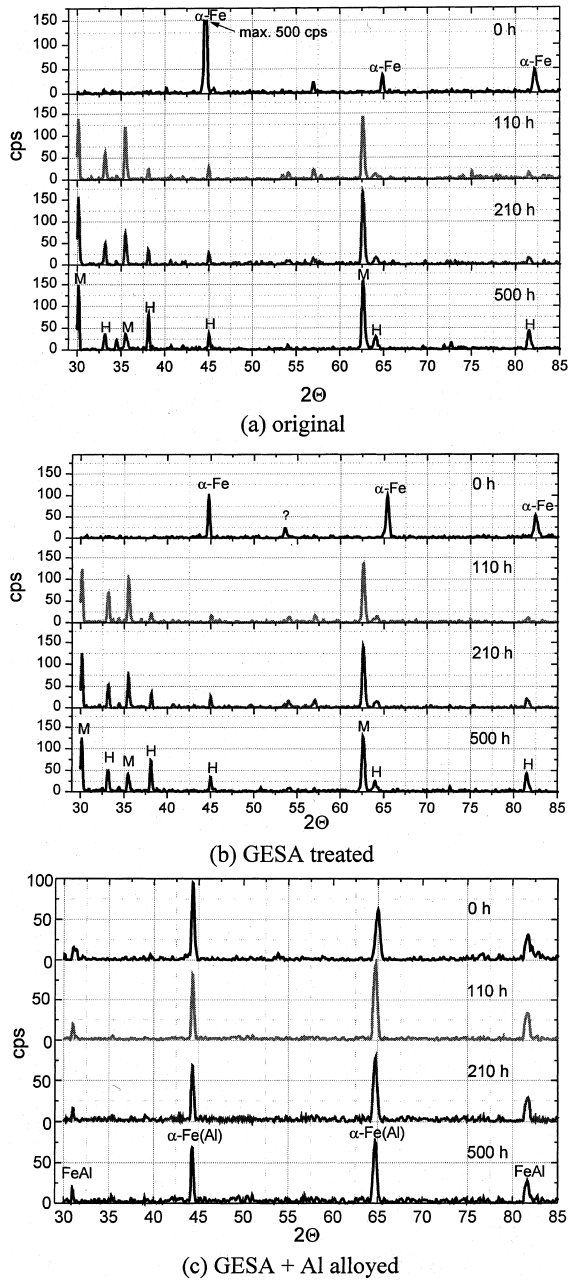

Fig. 9. X-ray diffraction patterns of OPTIFER specimens after oxidation at 550 °C in the corrosion test atmosphere with an H_2/H_2O ratio of 0.4. M = magnetite, H = hematite.

liquid lead containing 8×10^{-6} at.% oxygen consists in the practically Cr-free magnetite scale that develops on the steel–lead interface. This, however, corresponds to the preferred stratified scale type described by Whittle and Wood [15] for iron–chromium alloys with less than 18 % Cr. Since all their examinations are conducted in

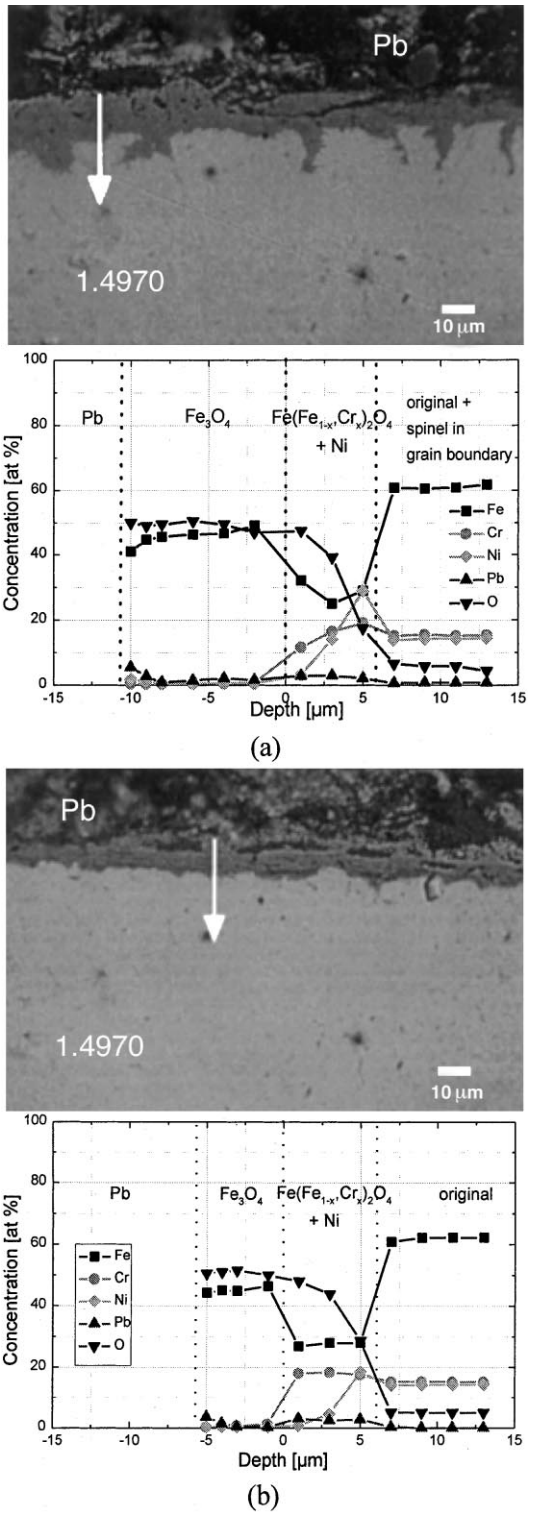

Fig. 10. SEM of the cross-section of 1.4970 specimens and EDX concentration profiles (at arrow position) after 3000 h at 550°C: (a) original A1, (b) GESA treated A2.

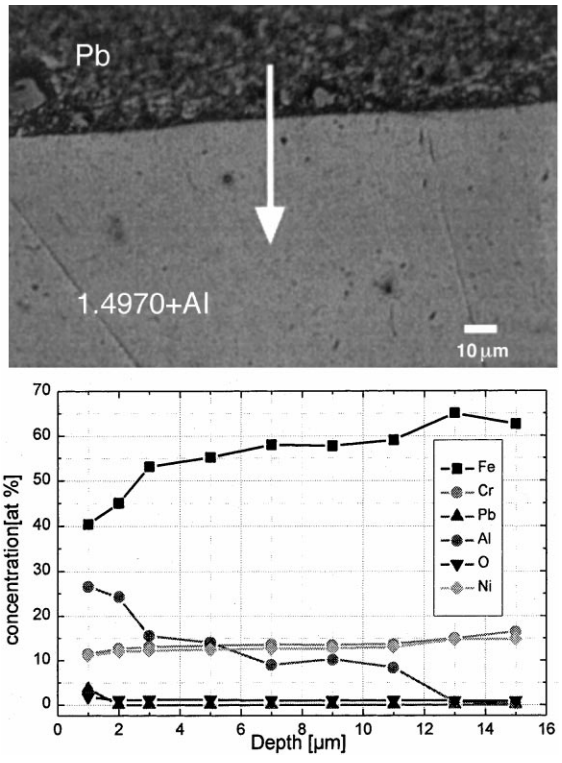

Fig. 11. SEM of the 1.4970 specimen alloyed with aluminum and EDX concentration profiles (at arrow position) after 1500 h at 550°C in liquid Pb.

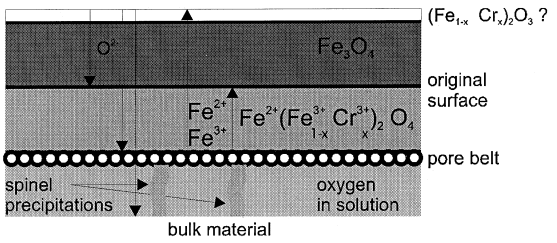

Fig. 12. Scheme of oxidation zones and ion migrations.

air, a small layer of hematite, Fe_2O_3, is formed on top of the magnetite layer. Our X-ray diffraction analysis shows indeed peaks that may indicate such a layer which could be stable from thermodynamic reasons in form of $(Fe_{1-x}Cr_x)_2O_3$. However, only up to 2% Cr are found in this region. Furthermore the diffraction lines are obtained from a scale grown in the test atmosphere under oxygen control and not exposed to liquid lead. Although this could explain the increase of oxygen concentration observed on top of the magnetite scale of OPTIFER steel specimens (Fig. 7(a) and (b)), further experiments and examinations are necessary to resolve the nature of the peaks.

Analogous to the oxidation mechanism described [13,14], anion as well as cation diffusion can be called responsible for the formation of the oxide layers. Oxygen penetrates the surface to form at first the Fe–Cr spinel that grows inwards, which agrees with investigations of Kuroda et al. [16]. Fe ions migrate to the surface, get oxidized and produce from there the magnetite scale that grows outward. This scale starts exactly at the surface and does not contain more than 1–2% of chromium. Oxygen migrates easily through the magnetite scale to the specimen surface, feeds the scale growth and partly diffuses into the spinel and solution zones. On the other hand, iron ions migrate through the magnetite layer and are oxidized on the surface of the magnetite scale. By these two processes, the magnetite scale grows from both sides as indicated in the scheme of the oxidation zones and migrating ions in Fig. 12.

There is no principal difference between the corrosion effects in lead and in the controlled furnace atmosphere at 550°C. Specimens exposed to the atmosphere show the same oxide structure as those in lead. Different are just the growth rate of the magnetite scale and spinel zone, and the fact, that no Ni depletion takes place in the spinel zone of the 1.4970 steel.

The behavior of 1.4970 steel specimens differs substantially from those of OPTIFER steel, although the stratified scale structure is the same. The magnetite scale is much thinner than that of OPTIFER steel, if it is visible at all. The same concerns the spinel and the diffusion zones with the exception of the deep grain boundary penetration of oxygen in the non-treated specimen A1 in Fig. 10(a). The low oxidation rates are caused by the higher oxidation resistance of high-alloyed steels [17].

As opposed to OPTIFER, the 1.4970 steel shows Pb-inclusions in the interface region between the magnetite scale and the spinel layer that reaches frequently into the spinel, Fig. 10(a) and (b). This effect depends obviously on the presence of Ni in the initial stage of scale formation when Ni is dissolved by liquid lead that gets trapped by the growing magnetite scale and solidifies with about 2 at.% Ni [5]. After this process the Ni depletion does not change any more with increasing exposure time. Thus, the Ni depletion zones in Fig. 10(a) and (b) represent the state established in the period before the first examination at 800 h of exposure.

The influence of electron pulse melting of a surface layer of the steels on the corrosion behavior in liquid lead at 550°C up to 3000 h exposure time is manifested in the following effects. In OPTIFER it causes a smaller magnetite scale and better spallation resistance of the spinel zone while in 1.4970 steel the deep grain boundary penetration of oxygen is avoided. The reason for this behavior is thought to be the finer grain structure in the

specimen surface layer after melting and rapid solidification. However, whether there will be a benefit of this effect for the corrosion behavior cannot yet be said with confidence. Tests with much longer exposure times and experiments in loops will be necessary to attain confidential statements.

In comparison of OPTIFER and 1.4970 steels, the austenitic material should be favored so far after 3000 h of testing, especially when the surface is treated by GESA. The corrosion zone consisting of the spinel layer and the diffusion zone is much thinner after that period. Fig. 13 shows the growth of the corrosion zones in both steels with and without surface treatment. The points represent the mean values of five measurements, each one obtained at a different position parallel to the surface. It indicates the better performance of 1.4970 steel with advantages for the surface treated specimen at least for the first 3000 h. No visible advantage of surface treatment can be observed for the OPTIFER specimen. The fragile magnetite scale is not considered in the evaluation because it constitutes a corrosion product that lies above the original specimen surface and is lost in the major part of the surface area. This effect will be enhanced by the flowing lead in loops.

The most striking effect is obtained with both OPTIFER and 1.4970 steels, when Al is alloyed into the surface layer during melting by GESA. The alumina layer that must have been formed at the surface during oxidation in lead with 8×10^{-6} at.% oxygen might be very thin and could not be detected up to now. However, it constitutes such an effective barrier against corrosion that not even a minimum attack occurred up to now after 1500 h. This agrees with investigations of the behavior of aluminized steel in liquid Pb–17Li in tests with 10 000 h exposure time [8] and with tests of the corrosion behavior of FeAl in liquid lead at 600°C [3].

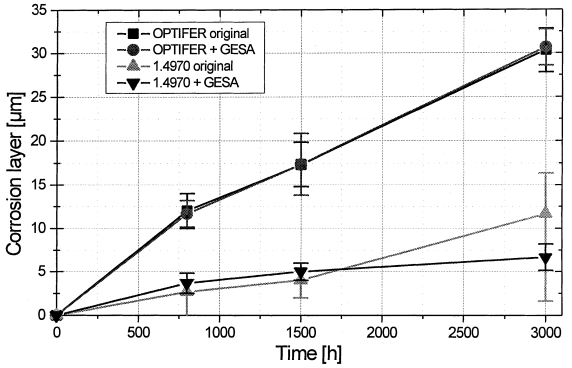

Fig. 13. Growth rate of the corrosion layers for original and GESA treated OPTIFER and 1.4970. The growth rate for Al-alloyed specimens is practically zero.

6. Conclusions

Oxide layers on steel can effectively prevent the steel from leaching of alloy components by dissolution in liquid lead. To maintain the oxide layers over long exposure time it is necessary to control the oxygen concentration in lead which can be done with a gas atmosphere of 10^{-22}–10^{-25} bar oxygen partial pressure. By this procedure the corrosion attack is changed from that of liquid metal corrosion to that of oxidation. Thus, it is needed to find materials that form stable protective oxide scales under controlled oxygen atmosphere in liquid lead.

Considering both the OPTIFER and 1.4970 steels, the austenite 1.4970 shows better resistance in liquid lead under oxygen control than OPTIFER. This is a consequence of the better oxidation resistance of 1.4970 steel. Electron pulse treatment improves the behavior of 1.4970 steel because it suppresses deep grain boundary penetration of oxygen due to the fine grained structure that forms by melting and rapid solidification. Alloying of aluminum into the surface by pulsed electron beam surface melting improves the corrosion oxidation behavior of both examined steel types in an impressive manner. No corrosion attack at all occurs after 1500 h of exposure.

Oxide scale formation under controlled gas atmosphere obeys the same principle mechanisms as in liquid lead with an oxygen concentration that corresponds to the same oxygen potential. Oxygen in liquid lead loops can be controlled by adjusted oxygen partial pressures which are effected, e.g. via hydrogen/water vapor or by electrochemical titration.

Findings in this work are just as well applicable to Pb–Bi loops. For application of the results to Pb and Pb–Bi loops, that run with controlled oxygen concentration to improve the corrosion resistance, it can be concluded that high alloyed oxidation resistant steels should be employed. Their properties can be improved by electron pulse treatment, especially when Al is alloyed into the surface by this process.

Acknowledgements

The work has been performed in the frame work of the Projekt Sicherheitsforschung of the Forschungszentrum Karlsruhe. The authors like to thank Ms Annette Heinzel for the analytical work and Mr Rolf Huber for conducting the corrosion experiments.

References

[1] C. Rubbia, J.A. Rubio, S. Buono, F. Carminati, Conceptual design of a fast neutron operated high power energy amplifier, CERN/AT/95-44 (ET), September 29, 1995.

[2] G.Y. Lai, High temperature corrosion of engineering alloys, ASM Int., Materials Park, OH 44073, 1990.
[3] R.C. Asher, D. Davies, S.A. Beetham, Corrosion Sci. 17 (1977) 545.
[4] B.F. Gromov, Yu.I. Orlov, P.N. Martynov, K.D. Ivanov, V.A. Gulevski, in: H.U. Borgstedt, G. Frees (Eds.), Liquid Metal Systems, Plenum, New York, 1995, p. 339.
[5] T.B. Massalski, (Ed.), Binary Phase Diagrams, 2nd Ed., ASM International, Metals Park, OH, 1990.
[6] C. Guminski, Z. Metallkd. 81 (1990) 105.
[7] R.P. Elliott, Constitution of Binary Alloys, First Supplement, New York, 1965.
[8] H.U. Borgstedt, H. Glasbrenner, Fusion Eng. Des. 27 (1995) 659.
[9] H. Kleykamp, H. Glasbrenner, Z. Metallkd. 88 (1997) 3.
[10] V. Markov, Seminar on the Concept of Lead-Cooled Fast Reactors, Cadarache, September 22–23, 1997 (unpublished).
[11] G. Müller, G. Schumacher, D. Strauß, Surface and Coating Technol. 108&109 (1998) 43.
[12] Landolt-Börnstein, Numerical Data and functional Relationships in Science and Technology, New Series, Group IV, vol. 5, Springer, Berlin, 1994.
[13] K. Hauffe, Oxidation of Metals, Plenum, 1965.
[14] D. Talbot, J. Talbot, Corrosion Science and Technology, CRC, Boca Raton, 1998.
[15] D.P. Whittle, G.C. Wood, J. Electrochem. Soc. 114 (1967) 986.
[16] K. Kuroda, P.A. Labun, G. Welsch, T.E. Mitchell, Oxidation of Metals 19 (3/4) (1983) 117.
[17] S.K. Mitra, S.K. Roy, S.K. Bose, Oxid. Met. 34 (1990) 101.